Multi-walled carbon nanotubes/PVDF blended membranes with sponge- and finger-like pores for direct contact membrane distillation

Tânia L.S. Silva, Sergio Morales-Torres*, José L. Figueiredo, Adrián M.T. Silva

LCM – Laboratory of Catalysis and Materials – Associate Laboratory LSRE-LCM, Faculdade de Engenharia, Universidade do Porto, Rua Dr. Roberto Frias, 4200-465 Porto, Portugal.

*Corresponding author: semoto@fe.up.pt (S. Morales-Torres).

Abstract

Polyvinylidene fluoride (PVDF) flat sheet membranes were blended with multi-walled carbon nanotubes (MWCNTs) by the phase inversion method for direct contact membrane distillation (DCMD) of salty water (35 g L^{-1} NaCl). The membrane properties and performances depended markedly on the synthesis parameters such as MWCNTs loading, polyvinylpyrrolidone (PVP) addition and MWCNTs surface chemistry. MWCNTs/PVDF membranes prepared with functionalized MWCNTs have a smaller pore size (determined by bubble point measurements) and lower contact angles, thus, functionalization of MWCNTs is not recommended for this application. For membranes presenting the same pore size, the pore morphology and the membrane thickness are crucial for efficient salt rejection. Sponge-like pores and the smallest possible thickness (i.e., membranes prepared without PVP) allow complete salt rejection (i.e., 100%), in contrast with larger thickness and elongated finger-like pores (resulting from PVP addition) whose salt exclusion ranged from 88.8 to 98.6%. Overall, the MWCNTs/PVDF blended membrane prepared with 0.2 wt.% optimal content of pristine MWCNTs (without adding PVP) exhibited the best performance in DCMD, presenting total salt rejection and a higher permeate flux (9.5×10^{-3} kg m^{-2} s^{-1}) than that obtained with a commercial PVDF membrane (7.8×10^{-3} kg m^{-2} s^{-1}).

Keywords: *carbon nanotubes (CNTs); polyvinylidene fluoride (PVDF); membranes; desalination; direct contact membrane distillation.*

1. Introduction

Water scarcity is among the main concerns to be faced by humankind in the 21st century. Growing population and economic expansion are the major factors affecting the availability of freshwater resources. Changes in production, consumption patterns, markets and politics have led to increasing domestic, industrial and agricultural water requirements [1]. Food security, industrial productivity, public health and environmental sustainability might be compromised if no technological improvements or policy changes are met. The adoption of technologies based on desalination can contribute for the development of alternative water sources and risk minimization.

Water desalination can be performed by several processes generally based on interactions with selective membranes, thermal distillation and/or application of electric fields [2]. Some of the conventional technologies include reverse osmosis (RO), electrodialysis (ED) or primary thermal distillation (TD) processes (such as multi-stage flash distillation, multi-effect distillation and thermal vapour compression), but RO is still the main route for water desalination. In particular, separation processes driven by improved membranes have received increasing attention from researchers, motivated by the needs in the industrial sectors. New technologies, such as membrane distillation (MD) and forward osmosis (FO), are seen as potential alternatives to the currently leading RO desalination technology. MD presents several advantages such as high rejection rates, theoretically total exclusion (100 %) of non-volatile solutes, low operating temperature and hydrostatic pressure and, thus, less demanding mechanical resistance for the membrane applied [3].

MD is a non-isothermal process based on the vapour pressure difference (driving force) resulting from the thermal gradient generated at both sides of a porous hydrophobic membrane, which prevents liquid water to enter into the pores until overcoming a specific pressure

difference, known as the liquid entry pressure (LEP). Thus, the membrane acts as a barrier through which only vapour molecules pass and then condensate on the permeate side. For this reason, low thermal conductivity (to avoid heat losses), high chemical resistance, good thermal stability, as well as appropriate pore size, thickness, surface roughness, hydrophobicity and porosity, are properties determining the membrane efficiency. Besides the membranes intrinsic characteristics, various operating parameters, such as feed temperature, flow rates, feed concentration, DCMD module design and respective hydrodynamic conditions, also determine the performance in MD processes [4-6]. For instance, Shirazi et al. [4] observed a higher permeate flux by increasing the flow rate of hot stream, the module depth on the cold side and the feed temperature, the last being the most important parameter in their study.

Direct contact (DCMD), sweeping gas (SGMD), vacuum (VMD) and air gap (AGMD) membrane distillation are the main MD configurations [3] and, among them, DCMD is the most frequently applied in lab-scale experiments, since it allows a better assessment of the membrane properties [7]. However, this technology has not yet been widely implemented at the industrial level due to challenges related with the module design, cost effectiveness, flux decay, permeate flow rate, possible membrane pore wetting, and energy efficiency when the process is not assisted using renewable sources of energy [8].

New research paradigms, involving the combination of nanotechnology and separation sciences, have resulted in promising solutions to overcome some of the membrane engineering issues. For instance, carbon nanotubes (CNTs) are an interesting option to improve the membrane performances due to their mechanical properties [9-11]. Compared to conventional MD membranes, the immobilization of CNTs in polymeric matrixes (e.g., polyvinylidene fluoride – PVDF), resulting in so-called mixed matrix membranes (MMMs), can reduce the required operating temperature of the MD process while increasing the water fluxes [12]. For instance, the beneficial effect of CNTs on MMMs has been reported for polyamide membranes,

and ascribed to the improved mechanical resistance of the membrane (toughness and tensile strength) and both salt and organic matter rejection [13]. Other studies dealing with self-supporting and supported CNTs membranes, known as buckypapers, have already demonstrated the successful application of CNTs membranes in DCMD for synthetic water desalination [14-17]. The CNTs membranes can have improved properties (i.e., high contact angle, high porosity and relatively low conductivity) when compared with most of the commercially available polymeric membranes applied in MD. Despite their remarkable properties, the CNTs tendency to form bundles by means of strong intrinsic van der Waals forces between the tubes [18], as well as their inert graphitic surface, may result in a poor interaction with the polymer when composites are prepared, in some cases limiting the CNTs effective dispersion.

In order to address this issue, CNTs edges and sidewalls can be functionalized, which in turns enhances the durability and stability of the membrane structure. Chemical functionalization of CNTs, by using treatments in gas or liquid phases, allows controlling the CNTs surface chemistry, some functional groups turning the surface more hydrophilic and, as consequence, improving their dispersion in specific solvents. This will also affect the membrane properties, promoting attractive or repulsive interactions depending on the target solute [19]. In our previous work [16], multi-walled carbon nanotubes (MWCNTs) were used to prepare buckypapers over a polytetrafluoroethylene (PTFE) commercial membrane. The resulting membranes were tested in DCMD under salinity conditions, a significantly enhancement on the permeate flux and a total rejection of chloride ions being observed when using functionalized CNTs instead of the pristine ones. In addition, a correlation between the permeate flux and the amount of oxygen functional groups of the MWCNTs was obtained.

In the present work, MWCNTs are used to prepare PVDF blended membranes, instead of buckypapers, studying different synthesis parameters such as the loading and surface chemistry

of the MWCNTs, pore former loading and PVDF molecular weight (M_W). The resulting MWCNTs/PVDF blended membranes are tested in DCMD of salty water and the membrane properties correlated with the performance obtained in terms of water permeation and salt rejection.

2. Experimental

2.1. Materials

Two different polyvinylidene fluoride (PVDF) polymers were used to prepare the membranes, one purchased from Alfa Aesar (Alfa Aesar® 44080, labelled as "A") and another kindly supplied by Solvay (Solef® 1015, labelled as "S"). Polyvinylpyrrolidone (PVP or P) was used as a pore former agent and 1-methyl-2-pyrrolidinone (NMP, anhydrous, 99.5 % and density of 1.03 g mL^{-1}) as solvent; both reagents were purchased from Sigma-Aldrich. Some physical properties of the PVP and PVDF polymers are collected in Table 1. NMP was used as solvent since it allows dissolving the PVDF polymer at a relative low temperature and because the CNTs dispersion (functionalized or pristine) was more effective in NMP than in other solvents, like *N,N*-dimethylformamide (DMF). In addition, the NMP toxicity is relatively lower than that of DMF. Pristine MWCNTs prepared by CVD were supplied by Nanocyl™ (NC3100 series). MWCNTs presented a carbon purity > 95 wt.%, outer diameter of 9.5 nm, average length of 1.5 μm and an ash content < 5 wt.%. Commercial PVDF membranes (GVHP Durapore® with 0.22 μm pore size, 125 μm of thickness and 25 mm of diameter) were purchased from Millipore and employed as reference.

Table 1. Properties of used polymers supplied by the manufacturers.

Nomenclature	Type of polymer	M_w (kDa)	Viscosity (Pa s)*	Density (g cm^{-3})	Melting point (°C)
"P"	Polyvinylpyrrolidone	10	NA	1.20	> 130
"A"	Alfa Aesar® 44080	~ 350	2350-2950	1.78	155-160
"S"	Solef® 1015	573	2800-3800	1.78	171-175

*Determined at 230 ºC and 100/s; NA – not available

2.2. Functionalization of carbon nanotubes

MWCNTs were oxidized by a HNO_3 hydrothermal method described in detail elsewhere [16]. In a typical oxidation experiment, 75 mL of a HNO_3 solution with concentration of 0.30 mol L^{-1} was transferred to a PTFE vessel and 0.2 g of MWCNTs was added. The PTFE vessel was placed into the stainless-steel autoclave (Parr Instruments, USA Mod. 4748) with 125 mL total volume, which was sealed and placed in an oven at 200 ºC for 2 h. After heat treatment, the autoclave was allowed to cool until room temperature. The recovered MWCNTs were washed several times using distilled (DI) water to remove the excess of acid until a neutral pH was achieved in the rising water, and then the samples were dried overnight at 120 ºC. The pristine and functionalized MWCNTs are labelled as MWp and MWf, respectively.

2.3. Preparation of membranes

MWCNTs/PVDF blended membranes were prepared by the phase inversion method containing different loadings of MWCNTs and PVP (as pore former), different MWCNTs surface chemistry (i.e., MWp and MWf) and different PVDF molecular weights.

In a typical procedure, an appropriate amount of MWCNTs (MWp or MWf) was dispersed in 60 mL of NMP for 10 min by using an ultrasonic processor (UP400S, 24 kHz) until achieving a uniform dispersion. In some cases PVP was added (2, 5 and 10 wt.%) as pore

forming agent. The PVDF polymer ("A" or "S") was degassed at 110 ºC under vacuum overnight before using and then dissolved (ca. 12 wt.%) in the NMP dispersion under continuous stirring at 70 ºC for 2 h to form a homogeneous casting solution. After that, the PVDF solution was cooled down and stored at room temperature overnight to remove the trapped air bubbles.

The degassed solution was subsequently casted on a glass dish through spin-coating (SPS-Europe, SPIN 150) at 3000 rpm for 1 s and then immersed immediately into a DI water coagulation bath at room temperature to induce the PVDF precipitation by a non-solvent/solvent (NMP/water) exchange and to form a homogenous membrane. Once the membrane was peeled off from the glass dish, it was transferred to another DI water bath and stored for at least 48 h to remove the residual solvent. Other authors have proposed this natural drying post-treatment of PVDF membranes to prevent the pore collapse [20]. Finally, the membrane was dried in air at room temperature and stored. Neat membranes were also prepared following the same experimental procedure but without any amount of MWCNTs.

The PVDF membranes prepared are labeled as follows: XY/W-ZP, where X is the amount of MWCNTs used (ranging from 0.1 to 1.0 wt.%); Y indicates the type of MWCNTs employed, i.e. MWp (pristine MWCNTs) or MWf (functionalized MWCNTs); W states the type of PVDF selected, i.e. "A" or "S" for Alfa Aesar or Solvay, respectively; ZP indicates the amount of PVP used (2, 5 and 10 wt.%). The nomenclature and composition of the prepared PVDF membranes are summarized in Table S1.

2.4. Membranes characterization

Membranes morphology was investigated by scanning electron microscopy (SEM) using a FEI Quanta 400FEG ESEM/EDAX Genesis X4M instrument (accelerating voltage of 15 kV and a working distance of ca. 10-15 mm).

Thermogravimetric (TG) and differential thermogravimetric (DTG) analyses of the membranes were performed using a STA 490 PC/4/H Luxx Netzsch thermal analyser, by heating the sample in nitrogen flow from 50 to 900 ºC at 20 ºC min^{-1}. Attenuated total reflection Fourier transform infrared (ATR-FTIR) spectra were recorded on a NICOLET 510P spectrometer. The membrane was pressed against a ZnSe crystal plate and all spectra were recorded from 4000 to 600 cm^{-1}.

The hydrophilicity of the membrane surface was determined by water contact angle measurements using DataPhysics (model OCA 15 Plus) and Attension (model Theta) equipments that allowed image acquisition and data analysis. The measurements were performed at room temperature, using the sessile drop method of water on dry membranes. Each contact angle was measured for at least 5 different locations on the membranes to determine the average value.

The overall porosity (ε) of the membranes was determined by the gravimetric method (Eq. 1), following a procedure similar to that reported by Smolders and Franken [21]. After measuring the dry weight of the membranes, they were immersed into isopropyl alcohol (IPA) overnight to assure the solvent penetration into the membrane pores and then their wet weight was registered.

$$\varepsilon\,(\%) = \frac{(m_w - m_d)/\rho_{IPA}}{(m_w - m_d)/\rho_{IPA} + m_d/\rho_p} \times 100 \qquad (1)$$

where m_w and m_d are the weights of the wet and dry membranes, respectively, and ρ_{IPA} and ρ_p are the IPA (0.786 g cm^{-3}) and polymer (1.78 g cm^{-3}) densities, respectively. Four membranes prepared by the same methodology were used to determine an average value of the porosity for each type of membrane, the standard deviation found being lower than ± 1 %.

N_2 adsorption-desorption isotherms at -196 ºC were obtained using a Quantachrome NOVA 4200e multi-station apparatus. The apparent surface area (S_{BET}) was determined by

applying the Brunauer–Emmett-Teller (BET) equation [22]. The volume of N_2 adsorbed at a relative pressure of 0.95 (V_{pore}) was also calculated from the adsorption isotherms, which corresponds to the sum of the micro- and mesopore volumes according to Gurvitch's rule [23-24].

The bubble-point method was used to determine the largest pore size of the membranes [25-26]. In this method, the pressure is slowly increased in one side of the membrane using a gas (nitrogen). When the liquid starts to leave the pores, gas bubbles can be observed on the permeating side of the membrane. The gas pressure required is typically known as bubble point. The largest pore diameter (d_{pore}) was calculated by Eq. 2:

$$d_{pore} = \frac{4\gamma cos\theta}{P_{bubble}} \quad (2)$$

where γ is the surface tension of the liquid (21.7 mN m^{-1} for IPA), θ is the contact angle of the liquid on the pore wall, and P_{bubble} (bar) is the bubble pressure. Three similar membranes were used to determine an average value of the bubble pressure for each type of membrane.

The membrane thickness was measured using an Absolute Digimatic Indicator (ID-F543, Mitutoyo Co., Japan). The membrane was placed on top of a highly softened granite surface and the height differences between the granite and membrane surfaces determine the membrane thickness. An average value was determined for each membrane by measuring different points of its surface.

2.5. Direct contact membrane distillation (DCMD)

The performance of all membranes, lab-prepared and commercial, was evaluated in a home-made DCMD unit (Figure 1), following a procedure reported elsewhere [16]. In a typical run, the membrane was placed into a "H-shaped" glass module operating in cross-flow

(effective membrane area of 2 cm^2). Then, salty (35 g L^{-1} of NaCl - feed) and distilled (DI - permeate) waters were pumped in recirculation mode through heat and cool exchangers, respectively, at similar flow rates (48 mL min^{-1}) for 60 min. The temperature at both sides of the DCMD module was continuously monitored by two thermocouples and maintained at 82 ºC (feed) and 20 ºC (permeate), resulting in a pressure difference of 54 kPa between both sides of the membrane. Ionic conductivity was measured in both feed and permeate streams by using online conductivity meters (VWR mod. 310) and ion chromatography (Metrohm, mod. 881 Compact IC pro) to determine the percentage of salt rejection. The permeate flux (J) of the membranes was calculated by Eq. 3:

$$J = \frac{\Delta W}{A \times \Delta t} \quad (3)$$

where J is the permeate flux (kg m^{-2} s^{-1}), ΔW is the mass of distillate (kg), A is the effective area of the membrane (m^2), and Δt is the sampling time (seconds). Experiments under the same experimental conditions were also performed using DI water at both sides of the membrane for 60 min. Solute rejection (R) coefficient was determined through Eq. 4:

$$R(\%) = 1 - \frac{C_p}{C_f} x100 \quad (4)$$

where C_p and C_f are the concentration of the permeate and the feed solution, respectively.

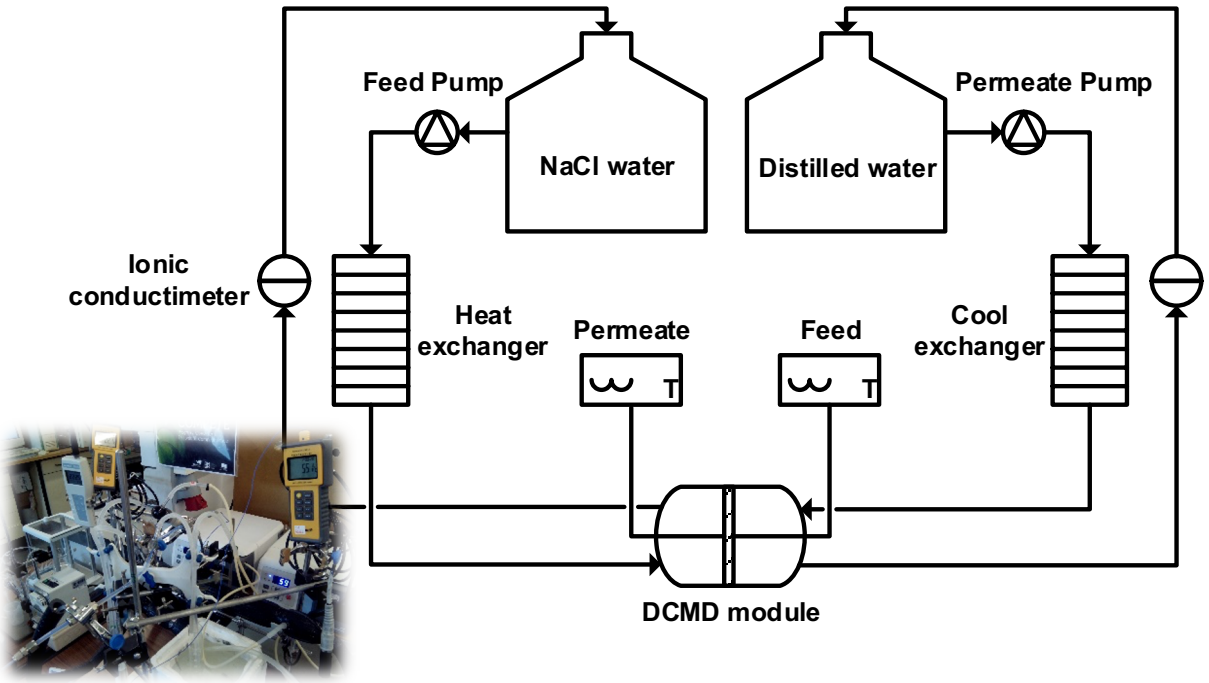

Figure 1. Schematic representation of the experimental DCMD set-up [16]. Reproduced by permission of the PCCP Owner Societies. Inset: original picture.

3. Results and discussion

3.1. Characterization of the membranes

3.1.1. Scanning electron microscopy (SEM)

The morphology of the neat membranes and of those modified with MWCNTs and PVP was studied by SEM. Figures 2 and 3 show representative SEM images of the top surfaces (at the same magnification) and cross-sections (at different magnifications), respectively. Regarding Figure 2, it can be observed that the incorporation of MWp, MWf and PVP obviously affected the porous structure of the corresponding membranes. Compared to the neat membrane "A" (Figure 2a), the surface topology of all other modified membranes generally exhibited a denser porous structure, originated by the presence of MWCNTs and PVP during the phase inversion process [27]. PVP obviously enhanced the formation of pores in both neat PVDF and MWCNTs/PVDF blended membranes (Figure 2b *vs* 2a and Figure 2e *vs* 2d/2c, respectively).

However, the surface pore density of smaller pores seems to be favoured for MWp loadings of 0.2 wt.% (Figure 2c). In comparison with MWp (Figure 2c), the use of functionalized MWCNTs (MWf) does not seem to favour the formation of pores (Figure 2d), even when they are added together with PVP (Figure 2f).

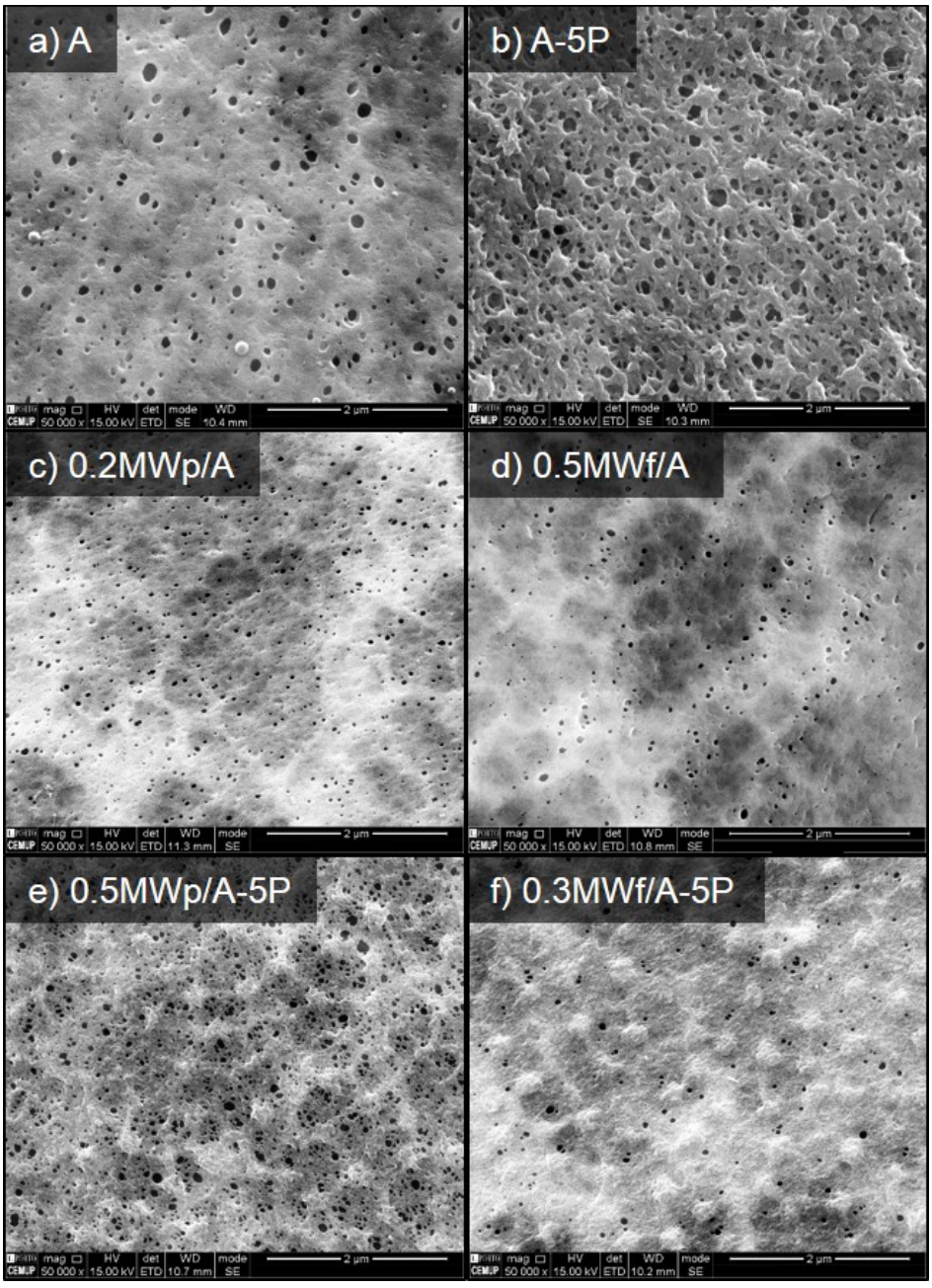

Figure 2. SEM micrographs of the top surfaces for selected neat PVDF and MWCNTs/PVDF blended membranes.

Thus, regarding the membrane top surface, the pores seem smaller and with higher density for the 0.2MWp/A sample (Figure 2c). In general, the mean pore size was in the range of 0.05-0.20 μm for the PVDF membranes, the lowest values (ca. 0.05-0.08 μm) corresponding to PVDF membranes blended with MWCNTs, for both pristine (MWp) and functionalized (MWf) carbon nanotubes, and the largest ones (0.15-0.20 μm) corresponding to neat PVDF membranes, including those prepared with PVP.

Regarding to the cross-section micrographs (Figure 3), the membranes presented a typical asymmetric structure consisting of a thin dense top-layer and a porous sub-layer/bulk morphology. PVP produced elongated finger-like pores across the membrane thickness (Figures 3b and 3g) due to the PVP solubility in water and, thus, its consequent removal from the polymer matrix when using the DI water coagulation bath to form the membrane [28]. For membranes modified with MWCNTs only (Figures 3c-3f and 3i), more evident morphology differences were observed in the sub-layer in comparison with the "A" membrane, namely sponge-like pores and macrovoids were formed, instead of elongated finger-like pores. Macrovoids are more likely to be formed in membranes modified with MWf, since oxygen functional groups can interact with the polymer chains, and in fact they were more notorious in Figure 3e. Isolated bundles of MWp were observed in the case of 0.2MWp/A, this membrane presenting sponge-like pores (Figures 3d and 3i). A good dispersion of MWf seems to be achieved for 0.5MWf/A, despite presenting higher MWCNTs loading (Figure 3f). In a study [29] performed with CNT/polyamide nanocomposite membranes, well-dispersed CNTs were also observed by SEM when CNTs were previously functionalized by acid treatments, and corroborated by Raman spectroscopy mapping and atomic force microscopy (AFM). On the other hand, when the PVDF membranes were prepared with both PVP and MWf, a more compact structure was obtained (Figure 3h). The overall porosity and pore sizes of all membranes are shown (Table 2) and discussed below.

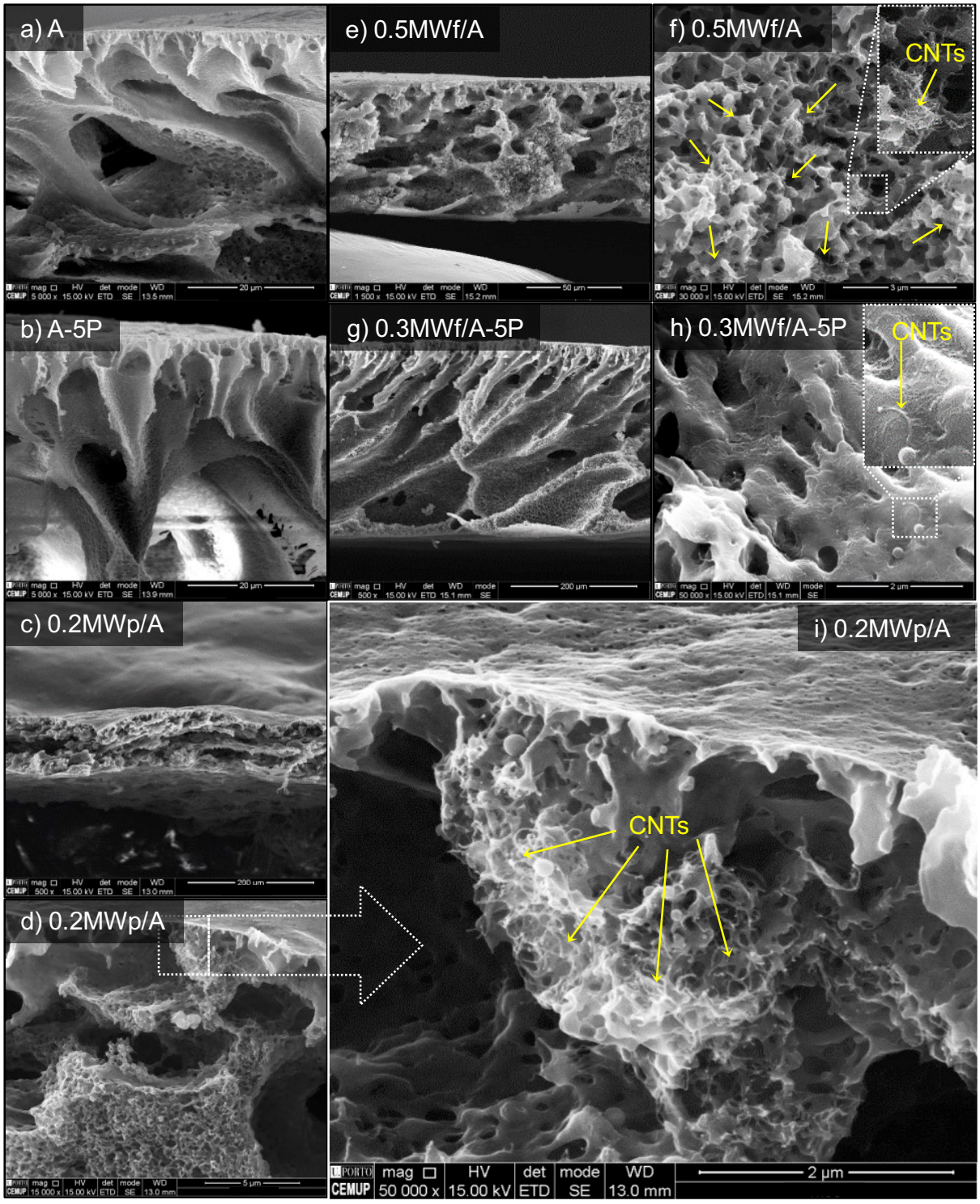

Figure 3. SEM micrographs of the cross-section for neat PVDF and MWCNTs/PVDF blended membranes (inset images with higher magnification).

3.1.2. Nitrogen adsorption isotherms, overall porosity, bubble point and contact angle.

The textural properties, namely the apparent BET surface area (S_{BET}) and the pore volume (V_{pore}), were determined by physical adsorption of nitrogen at -196 ºC. In general, the membranes did not present an appreciable development of the microporosity and mesoporosity, which is the typical range of porosity determined by this technique. However, some interesting correlations can be inferred from Figure 4.

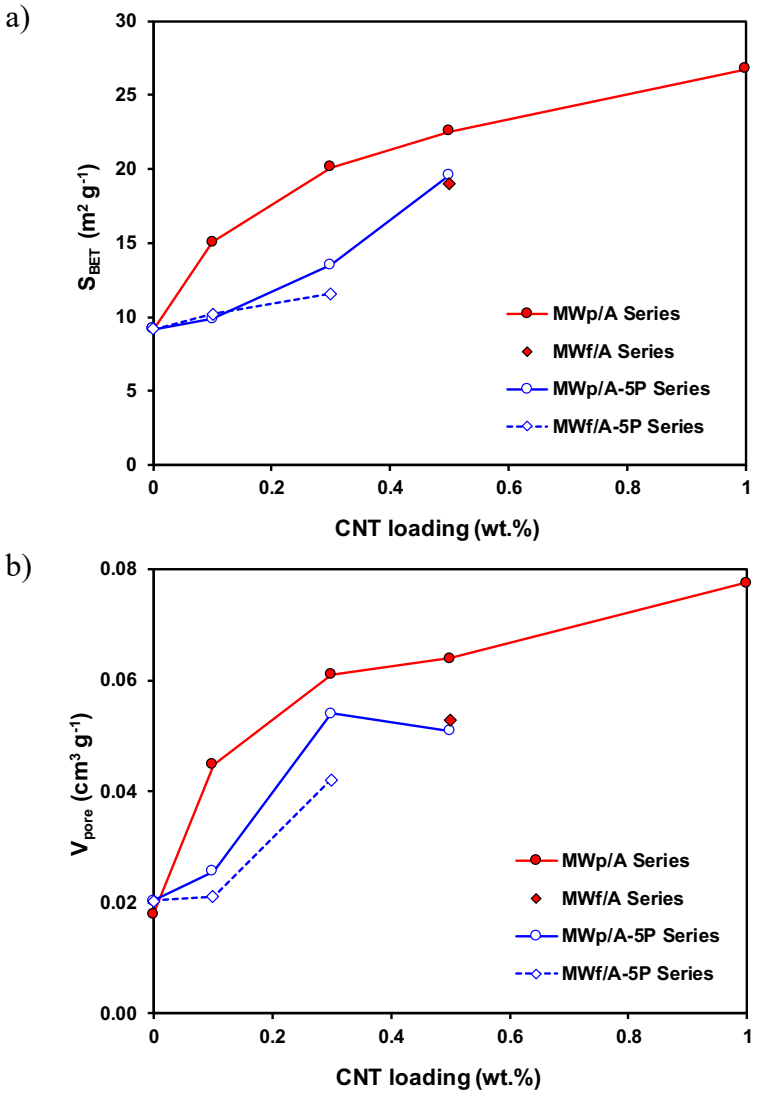

Figure 4. Dependency of the textural parameters: (a) apparent BET surface area and (b) pore volume, with the MWCNTs loading for MWCNTs/PVDF blended membranes. The data obtained for the neat membranes are also included as reference.

Neat membranes without MWCNTs (i.e., "A" and A-5P) presented the same low values of S_{BET} and V_{pore} (i.e., 9 m^2 g^{-1} and 0.02 cm^3 g^{-1}, respectively). A development of the porosity was generally observed with increasing MWCNTs loadings for all membranes modified with MWCNTs (e.g., S_{BET} = 27 m^2 g^{-1} for 1.0MWp/A). For both MWp and MWf, the increase of this type of porosity was more notorious in membranes modified with MWCNTs without PVP (e.g., S_{BET} = 20 and 14 m^2 g^{-1}, for 0.3MWp/A and 0.3MWp/A-5P, respectively). On the other hand, membranes with MWp showed higher S_{BET} and V_{pore} than those prepared with MWf, which can be attributed to the macrovoids formation observed for MWf (e.g., S_{BET} = 23 and 19 m^2 g^{-1}, for 0.5MWp/A and 0.5MWf/A, respectively). In general, the development of this type of porosity in the MWCNTs/PVDF blended membranes should be closely related to the MWCNTs dispersion and interactions established with the casting solution, which influence non-solvent/solvent exchange during the membrane formation and consequently, the porous structure.

The overall porosity was obtained by applying the gravimetric method (Table 2). The membranes obtained by the phase inversion method presented a high porosity, with values around 80-93 %, which were much higher than that obtained for the commercial PVDF membrane (GVHP), namely 62 %. Increasing the PVP loading slightly increased the porosity of the resulting membranes (e.g., 90 %, 91 %, 92 % for A-2P, A-5P, A-10P, respectively). This was also observed in membranes prepared with MWCNTs (e.g., 89 %, 91 %, 92 %, for 0.2MWp/A-2P, 0.2MWp/A-5P, 0.2MWp/A-10P, respectively). Membranes modified with MWCNTs only always presented lower porosity than the corresponding neat "A" membrane (e.g., 90 %, 88 %, 87 % and 73 %, for "A", 0.1MWp/A, 0.3MWp/A and 1.0MWp/A, respectively). In fact, the overall porosity seems to decrease with the MWp or MWf loading, which could be due to MWCNTs agglomeration in bundles or to the formation of macrovoids. Membranes prepared with the "A" polymer presented higher porosity than those prepared with

the “S” polymer (e.g., 90 % *vs.* 80 % for the neat “A” and “S” membranes, respectively; 86 % *vs.* 79 % for 0.2MWp/A and 0.2MWp/S membranes, respectively).

The largest pore size (d_{pore}) of the membranes, obtained by bubble point measurements (Table 2), also seems to be influenced by the MWCNTs loading and the MWCNTs surface chemistry, as well as the addition of different PVP loadings. For all membranes prepared, d_{pore} were always larger (> 2.0 μm) than that determined for GVHP (0.75 μm). In addition, the MWCNTs loading up to 0.2 wt.% of MWp leads to an increase of the membrane d_{pore} (up to 8.7 μm). The membranes with MWf presented smaller pores than those modified with MWp (e.g., 2.2 and 8.7 μm for 0.2MWf/A and 0.2MWp/A, and 3.5 and 4.3 μm for 0.5MWf/A and 0.5MWp/A, respectively). Finally, the amount of PVP also influences d_{pore}, smaller pores being obtained with higher PVP loadings.

Changes were produced not only on the physical properties of the membranes, but also on the surface hydrophobicity (Table 2). The incorporation of MWCNTs had different effects on the hydrophobicity of the membranes depending of their surface chemistry. In general, when MWp were used without PVP, the contact angle increased with the MWp loading (e.g., 88º, 92º and 94º for “A”, 0.3MWp/A and 1.0MWp/A, respectively), while a higher hydrophilicity was detected when using MWf (e.g., 88º, 84º and 83º for “A”, 0.2MWf/A and 0.5MWf/A, respectively). Membranes prepared with PVP generally showed lower contact angles than those prepared without PVP. However, it seems that the contact angle is quite similar when the MWCNTs content is fixed and the PVP load varied (e.g., 86º, 87º and 85º for 0.2MWp/A-2P, 0.2MWp/A-5P and 0.2MWp/A-10P, respectively). The M_W of the PVDF polymer influenced the contact angle since “A”-based membranes are often more hydrophobic than “S”-based membranes (e.g., 89º and 84º for 0.2MWp/A and 0.2MWp/S, as well as 92º and 88º for 0.3MWp/A and 0.3MWp/S, respectively). Therefore, the hydrophobicity of the membranes

depends on the chemical composition of the additives (CNTs and PVP) and can be also influenced by their surface roughness [30].

3.1.3. Thermogravimetric (TG/DTG) analysis

Figure 5 shows the TG/DTG curves obtained in nitrogen atmosphere for different MWCNTs/PVDF blended membranes and their corresponding neat membranes (i.e., "A" and A-5P). The PVDF polymer from Alfa Aesar decomposed at 480 ºC, as observed from TG/DTC curves of the "A" membrane (Figure 5a).

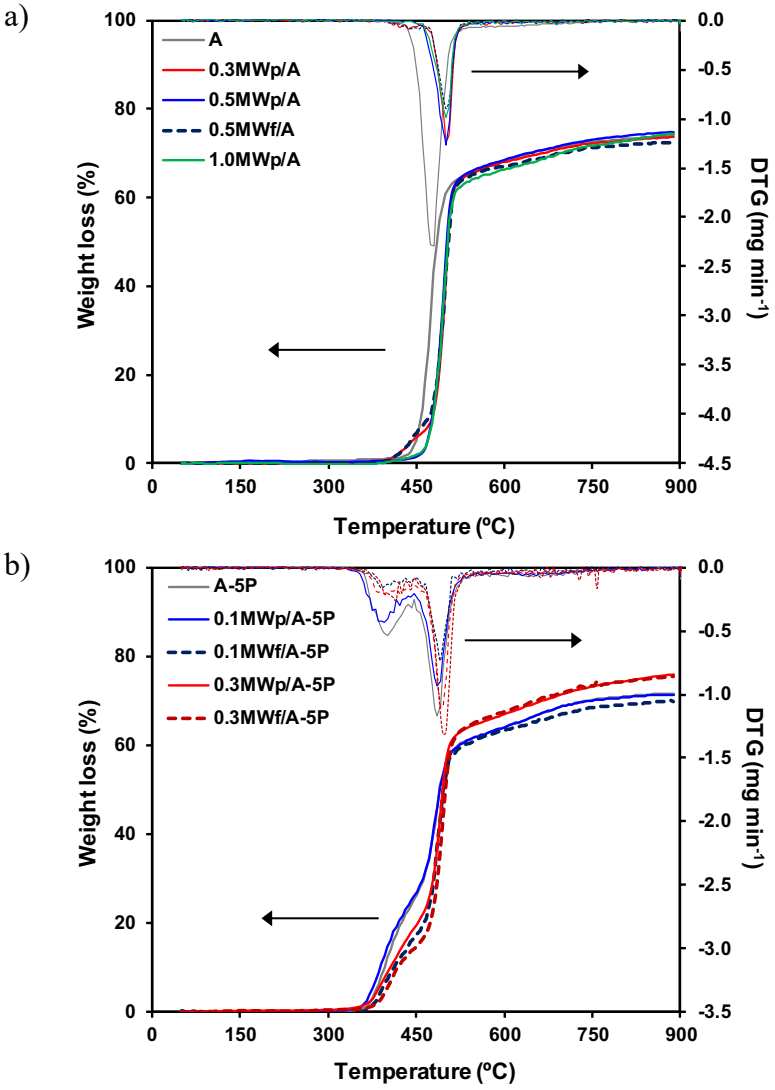

Figure 5. TG/DTG curves of MWCNTs/PVDF blended membranes and their corresponding neat membranes. (a) "A" series and (b) A-5P series.

Table 2. Porosity, contact angle, bubble pressure (P_{bubble}), pore diameter (d_{pore}) and thickness for all membranes (bold means the parameters that were changed in a set of experiments while keeping the others constant).

Membrane Label	Porosity (%)	Contact angle (°)	P_{bubble} (bar)	d_{pore} (μm)	Thickness (μm)
GVHP	62	119	1.15	0.75	125
"A"	90	88	0.35	2.5	258
"S"	86	88	0.40	2.2	365
A-**2P**	90	88	0.10	8.7	315
A-**5P**	91	90	0.15	5.8	317
A-**10P**	92	85	0.30	2.9	406
0.1MWp/A	88	91	0.30	2.9	412
0.2MWp/A	86	89	0.10	8.7	288
0.3MWp/A	87	92	n.d.	n.d.	322
0.5MWp/A	85	93	0.20	4.3	342
1.0MWp/A	73	94	n.d.	n.d.	435
0.2MWf/A	89	84	0.4	2.2	458
0.5MWf/A	80	83	0.25	3.5	231
0.1MWp/A-5P	90	78	n.d.	n.d.	355
0.2MWp/A-**2P**	89	86	0.10	8.7	464
0.2MWp/A-**5P**	91	87	0.15	5.8	388
0.2MWp/A-**10P**	92	85	0.20	4.3	453
0.3MWp/A-5P	91	80	n.d.	n.d.	368
0.5MWp/A-5P	90	81	0.15	5.8	873
0.1MWf/A-5P	92	86	n.d.	n.d.	554
0.3MWf/A-5P	91	81	0.30	2.9	302
0.2MWp/S	79	84	n.d.	n.d.	264
0.3MWp/S	84	88	0.15	5.8	139
0.3MW**f**/S	84	82	0.35	2.5	406

n.d.: not determined.

In the case of the corresponding membranes prepared with MWCNTs/A, the degradation temperature increased up to 501 ºC, thermal stability of the matrix being obtained due to the addition of MWCNTs, regardless of the amount of MWCNTs used and their surface chemistry. In general, the thermal stability of MWCNTs/PVDF blended membranes is directly related with the dispersion state and the loading level of MWCNTs [31]. In the case of "A"-based membranes modified with 5 wt.% of PVP, two weight loss steps were clearly observed, at 401 and 486 ºC, due to the decomposition of PVP and PVDF, respectively (Figure 5b). The incorporation of MWCNTs into the polymer matrix seems also to improve the thermal stability of the resulting membranes, but the enhancement is not as notorious as in the case of the membranes without PVP.

3.1.4. Surface analysis (ATR-FTIR)

ATR-FTIR analysis was used to obtain insights on the chemical interactions between the PVDF polymer and functionalized MWCNTs. Figure 6 shows the ATR-DRIFT spectra for two membranes ("A" and 0.2MWf/A membranes). In comparison with the spectrum of "A", the spectrum of the 0.2MWf/A membrane shows a band centred around 1666 cm^{-1}, which is characteristic of the C=O stretching vibrations of the –COOH groups incorporated in MWf [27]. The strong peak at 1402 cm^{-1} corresponds to C–F stretching vibrations, while the C–C band is clearly observed at 1182 cm^{-1} [32].

3.2. Direct contact membrane distillation (DCMD)

The DCMD experiments were performed with DI and salty water at the same operating conditions (i.e., Tf = 82 °C, Tp = 20 °C, flow rate of feed and permeate sides = 48 mL min^{-1}). Besides the water flux, the salt rejection was registered in experiments with salty water and represented in Figures 7-11.

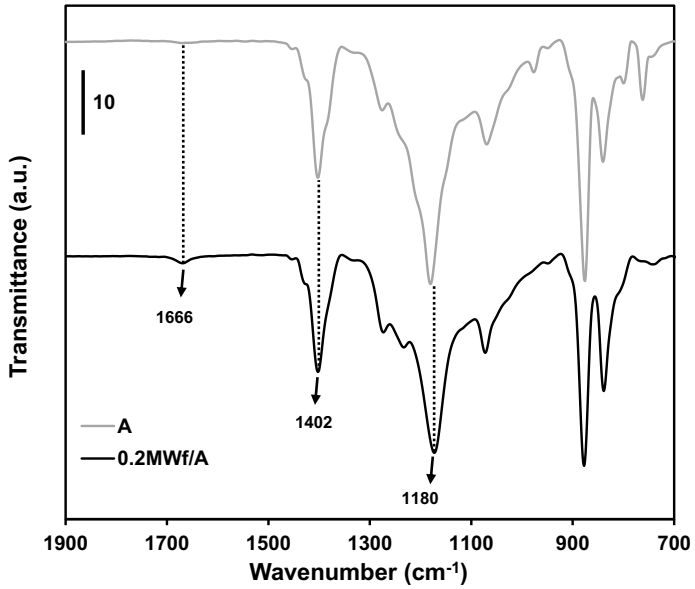

Figure 6. ATR-FTIR spectra of neat "A" and 0.2MWf/A membranes.

3.2.1. Preliminary studies with the prepared membranes

Preliminary experiments to assess the effect of active layer orientation, coagulation bath composition and backing structure addition were performed. Asymmetric membranes are known for having a thin top layer over a porous substructure or backing material. The first layer acts as the selective barrier and the porous sub-layer offers mechanical strength to the membrane [33]. Membrane porosity, tortuosity, thickness and pore size are the main factors determining membrane performance. However, in case of DCMD applications for water desalination, the high selectivity involves the maintenance of an air-gap formed inside the membrane [34]. In fact, this vapour layer will shrink to a point where the membrane will be soaked in water if a more hydrophilic material is used, leading to the formation of direct bridges between feed and permeate and lowering its selectivity. Dumée et al. [34] evaluated the influence of surface energy on membrane performance in DCMD, showing an increase in permeation for the membranes with higher contact angles and suggesting a reduction in heat transfer as possible explanation.

In the present work, some of the membranes presented a very high contact angle at the bottom surface compared to the top side (116° and 92º, respectively for 0.3MWp/A). Thus, an experiment with 0.3MWp/A was performed in order to investigate the influence of the layer orientation in DCMD (Figure 7). The labels ALFS and ALPS indicate "active layer feed side" and "active layer permeate side" conformations, respectively. Figure 7 shows a decrease of the flux for 0.3MWp/A placed with the bottom surface facing the feed side solution (ALPS). This may be related to an increase in the resistance of vapour molecules diffusion caused by the denser structure of the sub-layer and a larger membrane tortuosity, which should be as small as possible, since it is inversely proportional to membrane permeability [33]. On the other hand, the pore size, pore density, hydrophobicity and roughness of the active skin layer determines the selectivity (i.e. salt rejection) and permeability of the membrane when using the ALFS configuration, and they have less importance when ALPS configuration is used. Therefore, the high hydrophobicity of the bottom surface did not improve the flux and the contact angle determined might be influenced by the surface roughness and complex textures [35].

Regarding the coagulation bath composition, a membrane was prepared by using a water/isopropyl alcohol solution (70:30 v/v) instead of DI water only. When evaluating the performance of the 0.3MWp/A membrane obtained with each type of coagulation bath, a flux decline was found for the membrane obtained with the isopropyl alcohol solution (0.3MWp/A OH), as shown in Figure 7. This decrease of the performance could be related with the lower porosity obtained for 0.3MWp/A OH compared to 0.3MWp/A (i.e., 80 % and 87 %, respectively).

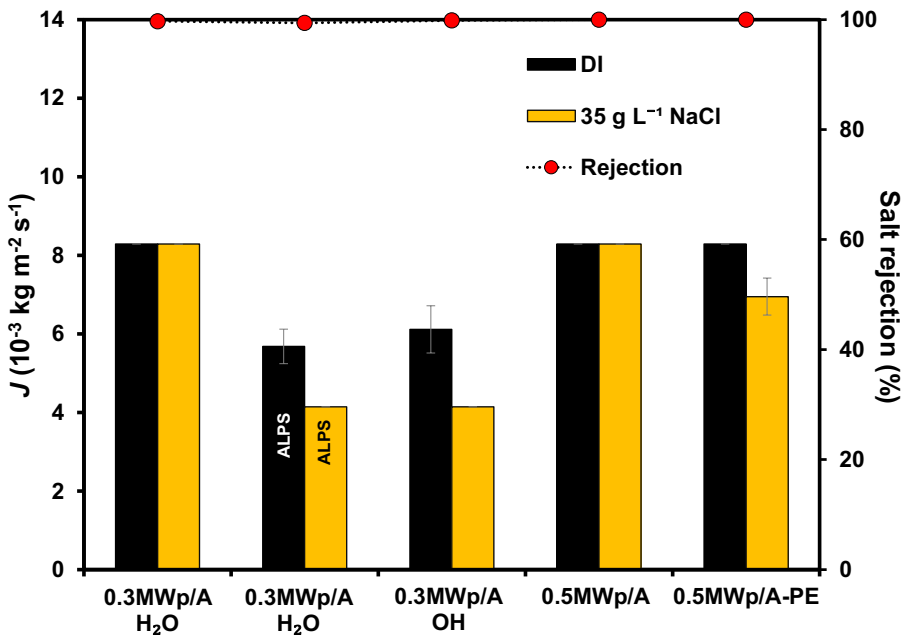

Figure 7. Effect of top layer orientation (ALFS - active layer feed side, and ALPS - active layer permeate side), coagulation bath composition (H_2O – water, and OH – water/isopropyl alcohol 70:30 v/v) and polyester (PE) nonwoven support on permeate flux and salt rejection in DCMD.

The backing structure morphology also plays an important role in membranes properties such as permeability and thermal efficiency. The support layer is responsible for providing a stronger mechanical resistance and softening the impact of flux variations and hydraulic disturbance. The present investigation involved the preparation of PVDF flat sheet membranes layered on a polyester (PE) nonwoven support (0.5MWp/A-PE), forming a so-called dual face hydrophobic/hydrophilic composite membrane. Figure 7 shows the permeate flux values achieved for non-supported 0.5MWp/A and supported 0.5MWp/A-PE. Only small differences of permeate fluxes were detected with salty water. According to Winter et al. [36], if the support layer is facing the permeate side, the flux and thermal efficiency deviations are low, in agreement with the negligible differences that were observed in terms of permeability and salt rejection when both supported and unsupported membranes were tested. This demonstrates that membranes with stronger mechanical resistance and longer lifetime, while maintaining their

permeability and salt rejection, can be produced by using polyester nonwoven supports, of relevance for membrane distillation applications at an industrial level.

3.2.2. Effect of PVP

Membrane performance is generally determined by its porosity, pore interconnection, pore size and hydrophobicity. The effect of different amounts of the hydrophilic pore former additive (PVP) on the performance of the resulting PVDF membranes was evaluated. PVP is a non-toxic hydrophilic material (as confirmed by the lower contact angles when PVP was used, Table 2) whose addition often results in an influx of non-solvent during the inversion phase method [37], being dissolved out in water and giving rise to the formation of finger-like pores (in contrast to the addition of MWCNTs only, as previously observed in Figure 3).

Figure 8a shows the effect of increasing PVP content (from 2 to 5 and 10 wt.%) on permeate flux and salt rejection of the prepared PVDF membranes (A-P), in experiments performed with DI and salty water. The increment in the PVP content from 0 to 2 wt.% gave rise to an almost eightfold permeate flux, but also caused a serious decrease in salt rejection (from 99.8 % to 78.3 % for the neat "A" and A-2P membranes, respectively). This can be ascribed to the largest pore diameter of these membranes (2.5 and 8.7 μm for "A" and A-2P, respectively, Table 2). Higher PVP increments resulted in a lower membrane permeability, but the salt rejection was maintained around 99 %. The decrease of the membrane permeability by PVP addition could be due to the smaller pore size diameters obtained for higher PVP contents and/or to the higher membrane hydrophilicity, confirmed by the lower contact angles measured (ranging from 88° to 85°). The membrane hydrophobicity is crucial for the MD application, preventing membrane wetting and so reducing the temperature polarization effect [33]. In general, the presence of additives can result in two opposite effects: (i) to increase the casting solution viscosity and, consequently cause a delay in the casting precipitation, favouring the

formation of a denser structure and less permeable membrane; (ii) to accelerate the phase inversion process, causing an instantaneous phase inversion that promotes the formation of macrovoids and finger-like pores [38-39].

Saljoughi et al. [40] reported that an increase from 0 to 1.5 wt.% in PVP loading in cellulose acetate (CA) membranes promoted the formation of a porous sub-layer, reducing flux resistance and, therefore, rising pure water flux (PWF), but also decreasing solute rejection. Further PVP increments (from 1.5 to 3.6 and 9 wt.%) were responsible for a gradual decrease of macrovoids development [40], resulting in a decrease in permeate flux while increasing salt rejection rates. In the present work, increasing PVP loading always resulted in a continuous increase of membrane porosity. However, for the membranes including 5 and 10 wt.% of PVP, smaller pores were formed and lower contact angles were measured, which may have determined the lower permeate fluxes obtained.

Figure 8b exhibits the effect of the PVP content on the performance of a PVDF membrane blended with 0.2 wt.% of MWp. The overall flux behaviour is similar to that previously observed for membranes without MWCNTs; however, a significant increase in permeate flux was found for the membrane prepared with 2 wt.% of PVP when tested with the 35 g L^{-1} feed solution. This may be due to a certain membrane wetting over time. Therefore, around 5 wt.% of PVP seems to be the optimum value to obtain PVDF membranes with high permeability and practically total salt rejection. Nevertheless, salt rejection is not 100% as in the case of the 0.2MWp/A membrane, suggesting that this membrane is more appropriate for DCMD that the others shown in Figure 8.

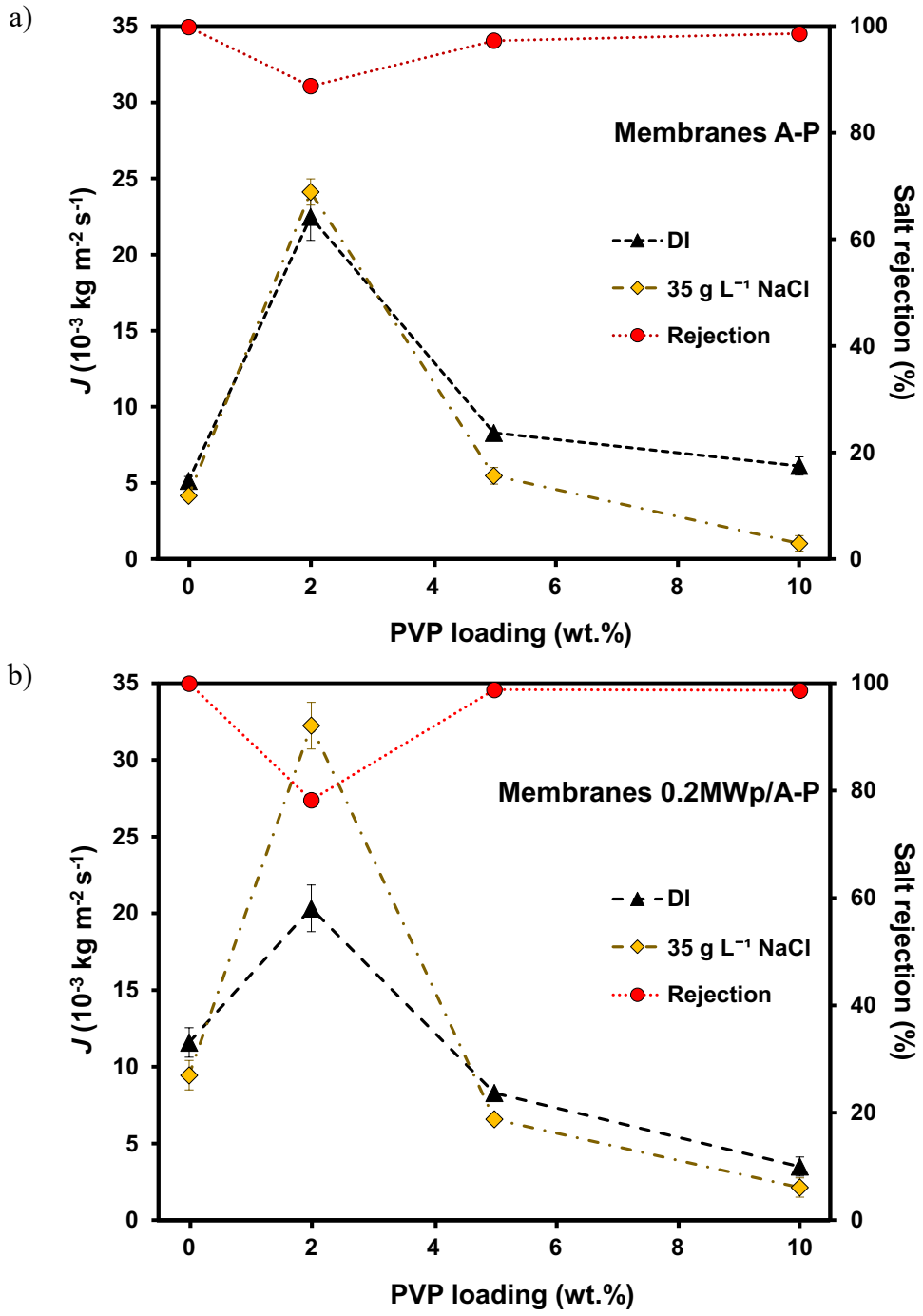

Figure 8. Effect of PVP loading on permeate flux and salt rejection for (a) A-P and (b) 0.2MWp/A-P blended membranes in DCMD.

3.2.3. Effect of MWCNTs loading

MWCNTs have already been used to improve the performance of membranes in separation applications [41-43]. Namely for water desalination, Bhadra et al. [19] reported a 50-77 % enhancement of the mass transfer coefficient with the immobilization of MWCNTs into PVDF membranes, MWCNTs acting as transporters of molecules and also as sorbent sites for vapour [41], which ends up increasing the overall membrane permeability while increasing also its selectivity [44].

In the present study, different amounts of MWp in the polymer matrix were investigated, through a gradual increase of MWp content in a range of 0 to 1.0 wt.%. Figure 9a shows the permeated flux obtained with increasing MWp loading, while Figure 9b represents the same influence but in this case with additional PVP inclusion. The first important conclusion is that the membranes prepared without PVP (Figure 9a) allow obtaining 100% salt rejection, in contrast with those prepared with PVP (Figure 9b). Therefore, the membranes prepared without PVP are more promising for DCMD, since the concept of the process is based on 100% selectivity to water vapour molecules (i.e., complete exclusion of non-volatile solutes).

Figure 9a also shows that the addition of any amount of MWp improves the water flux compared to the neat "A" membrane, without affecting salt rejection. The PVDF membrane containing 0.2 wt.% of MWp (sponge-like pores, Figures 3d and 3i) is the most efficient, water flux increasing more than twice when compared to the neat PVDF membrane (i.e., from 5.1×10^{-3} to 11.6×10^{-3} kg m^{-2} s^{-1} with DI water, and from 4.1×10^{-3} to 9.5×10^{-3} kg m^{-2} s^{-1} with salty water). The 0.2MWp/A membrane also presented a superior performance in comparison to the commercial PVDF membrane (GVHP), regarding both DI and salty waters, in spite of having a lower hydrophobicity (Table 2). However, the inclusion of a MWp content above 0.2 wt.% into the membrane matrix seems to decrease its permeability.

a)

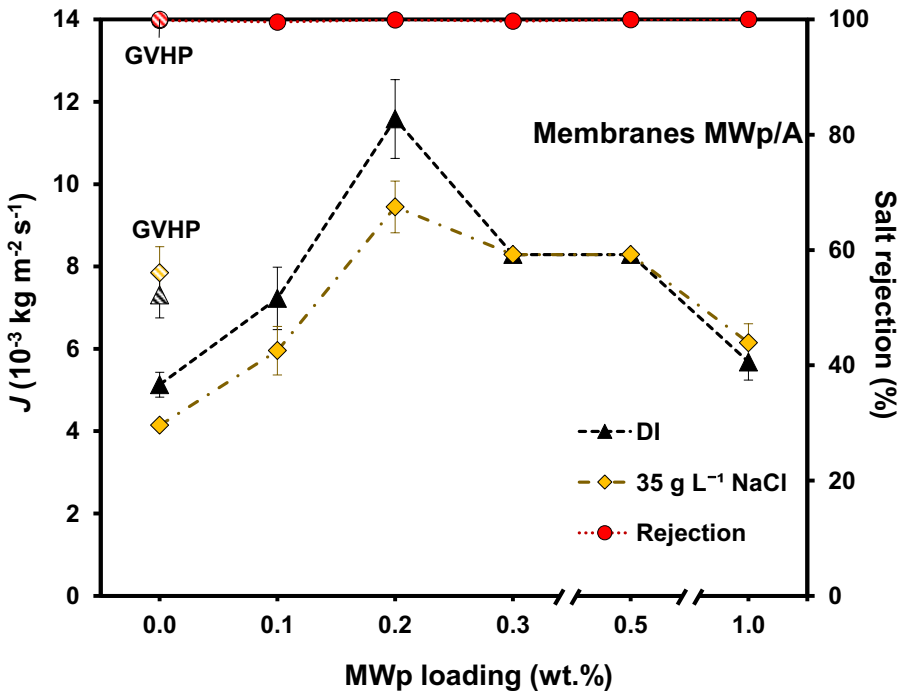

b)

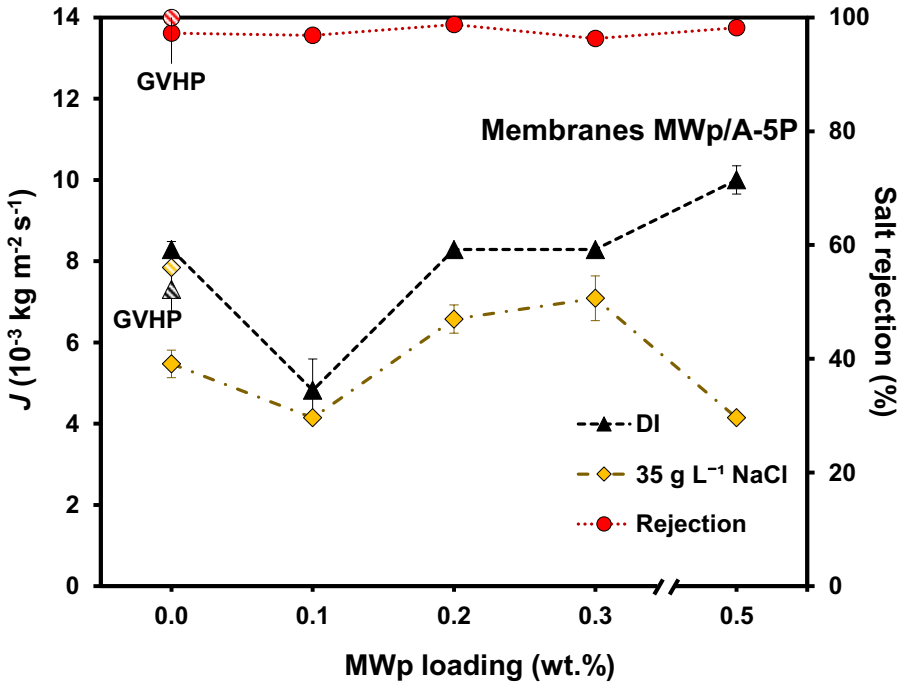

Figure 9. Effect of MWp loading on permeate flux and salt rejection for (a) MWp/A and (b) MWp/A-5P blended membranes in DCMD. Data corresponding to the commercial GVHP membrane are included for comparison.

Other studies also reported an increase of flux and salt exclusion up to a certain optimum value after which no further enhancement was observed [19]. MWCNTs immobilization into mixed matrix membranes is reported to alter water-membrane and solute-membrane interactions, which may determine their permeability and selectivity [45]. Their hydrophobic nature reduces the tendency of pore wetting, and so higher fluxes of vapour may occur. Another important aspect is their high sorption and desorption capacity and smooth surface, which may favour the interaction of vapour molecules with MWCNTs, allowing them to move from one point to another by a surface diffusion pattern [45], thereby increasing overall vapour transport through the polymeric membrane. In addition, MWCNTs exhibit high thermal conductivity which may help reducing the condensation rate inside the membrane, therefore allowing vapour to pass freely through its pores.

Sequential increments of MWCNTs content higher than 0.2 wt.% resulted in flux reduction, as already mentioned. An explanation could be the poor dispersion of high contents of the non-functionalized MWCNTs in the NMP solvent used to prepare the membranes. High MWp contents favour the interactions between nanotubes, giving rise to bundles (as observed by SEM analysis) and, therefore, reducing polymeric chain mobility and significantly affecting the rheological characteristics of the obtained composites [46]. In fact, the higher MWp content resulted in a decrease of the membrane porosity and the largest pore size (Table 2), which seem to be key factors determining water flux [47].

In Figure 9b the same tendency of increasing flux with the MWp content (up to a certain value of 0.2-0.3 wt.% with salty water) is observed for membranes containing 5 wt.% of PVP. In this case, only the membranes with 0.2 and 0.3 wt.% of MWp presented better performances than the A-5P membrane in salty water conditions. However, the salt rejection was always lower than 100%. Therefore, in general, PVP addition produced membranes with higher thickness (355-873 μm instead of 288-435 μm without PVP), inducing finger-like pores and a

decrease of hydrophobicity regardless the MWp content (Table 2). These characteristics are not interesting for DCMD because the water flux decreases and the salt rejection increases when using PVP, as also observed above in studies with a fixed amount of MWp (0.2 wt.%).

3.2.4. Effect of CNT functionalization

The addition of MWCNTs as fillers in the PVDF polymeric matrix has already proven to modify significantly the membrane performance. However, high MWCNTs contents led to a poor dispersion and the formation of agglomerates. To improve the dispersion of MWCNTs, different non-covalent and covalent modifications may be applied. The most commonly adopted method includes MWCNTs surface treatment using strong inorganic acids [48]. In this context, a HNO_3 hydrothermal oxidation methodology developed by our group was selected for MWCNTs functionalization [16, 49-50].

Figure 10a shows an improvement of permeability for the neat "A" membrane (0 wt.% of MWCNTs) when MWf are added, a 38 % increase in pure water flux being achieved for the membrane including 0.2 wt.% of MWf (i.e., 4.14 and 7.71 × 10^{-3} kg m^{-2} s^{-1}, respectively). On the other hand, when comparing the overall performances of the membranes prepared with MWf (Figure 10a) to those obtained with MWp (Figure 9a), the introduction of MWf instead of MWp resulted in a flux decrease. This behaviour seems to be related with the smaller pore size and lower hydrophobicity observed for membranes prepared with MWf in comparison with those prepared with MWp. The addition of functional groups to the edges and sidewall defects of MWCNTs was reported as responsible for enhancing the interfacial adhesion between MWCNTs and the membrane polymer [11], which was also proved (Table 2) to decrease the overall membrane hydrophobicity.

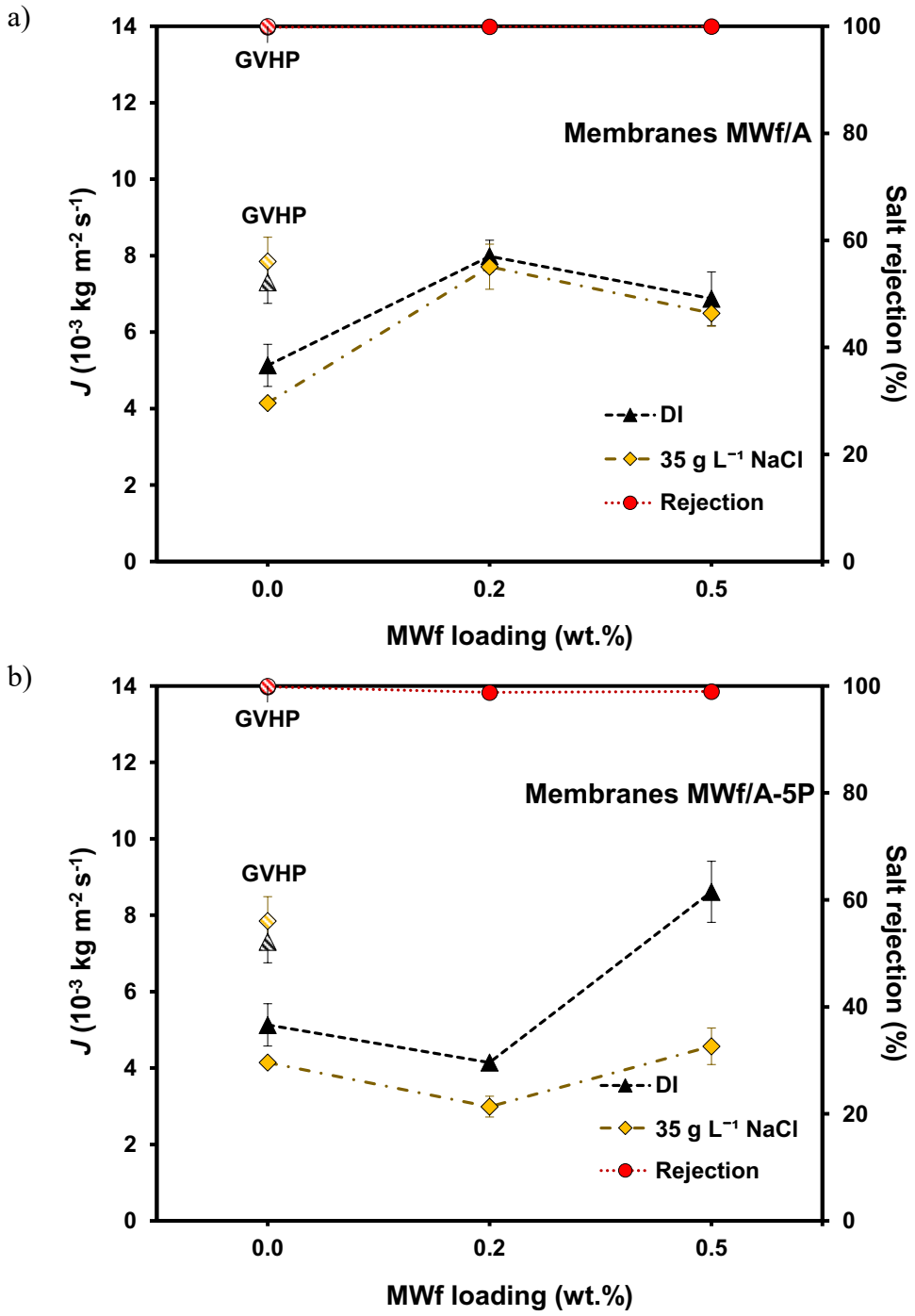

Figure 10. Effect of MWCNTs surface chemistry on permeate flux and salt rejection for (a) MWf/A and (b) MWfA-5P blended membranes in DCMD. Data corresponding to the commercial GVHP membrane are included for comparison.

The determining effect of MWCNTs surface chemistry was already described in our previous work [16]. Dumée et al. have shown that, for membranes exhibiting similar geometric

properties (pore size and porosity), the vapour permeation was seriously enhanced in membranes with low surface energy (i.e. more hydrophobic, as shown by higher contact angles) [34]. In our case the combination between the lower porosity and pore size found for the MWf modified membranes and the more hydrophilic character may have determined the reduced membrane permeability. The pore architecture of the membranes prepared with MWf was also slightly different (Figure 3e), showing more macrovoids and higher tortuosity, which may cause an additional resistance to the vapour diffusion. Corry [51] also suggested a steric blockage of the membrane pores by the functional groups or by ions (Na^+ or Cl^-) that can be attracted to them creating clusters (if charged groups are included, e.g. NH_3^+ or COO^-) and that may cause a decrease in the pore entrance area of the MWCNTs blended membranes.

Lower permeate fluxes may be also related with the increasing viscosity of the casting solutions when including functionalized MWCNTs. Ramana et al. [52] reported a drastic increase in the viscosity for the composites containing functionalized MWCNTs when compared to the original pristine nanotubes, for the same filler content. The presence of several bonding sites between MWCNTs and the polymeric substrate results in the formation of a complex network. A lower thermodynamic stability of the casting solution, caused by the introduction of the more hydrophilic MWCNTs, together with steric obstructions and electrostatic interactions between the functionalized MWCNTs and the polymeric matrix play a major role in the final membrane morphology and overall performance [47].

Figure 10b shows the influence of MWCNTs surface chemistry on permeate flux of membranes containing 5 wt.% of PVP. Once again, the general predominant negative effect of adding PVP is observed, regardless of the carbon content, MWf leading to lower water fluxes in experiments with salty water. It is noteworthy that the use of PVP in PVDF membranes produced a slight decrease in salt rejection, but the addition of MWf seems to improve it. The beneficial effect of MWf for buckypapers supported on polytetrafluoroethylene membranes

was already reported and explained by the creation of repulsive electrostatic interactions established between the chloride ions and the negatively charged surface of the buckypapers [16]. This effect is not so notorious in the present work since the nanotubes of MWf seem to be mostly interacting with the polymer in the MWCNTs/PVDF blended membranes, while in buckypapers the nanotubes are in direct contact with the fluids.

3.2.5. Effect of polymer molecular weight

The polymer molecular weight (M_W) is a parameter defining final membranes morphology and performance [37, 39, 53-54]. The viscosity of a casting solution depends strongly on the polymer M_W, determining the amount of segment-segment linkages between molecules [53].

In order to assess the effect of the polymer Mw on water flux and salt rejection in DCMD performance, a PVDF polymer supplied by Solvay (Solef® 1015, labels as "S") was also used to prepare a few membranes. The two polymers tested in the present work exhibit different physical properties (Table 1), one presenting medium viscosity ("A") and the other high viscosity ("S"). No significant differences are registered between the obtained permeate fluxes for the neat membranes (Figure 11); however a slight decrease in the overall performance with the "S" membrane can be justified by the lower membrane porosity (Table 2), i.e. 90 % for "A" and 86 % for "S", and pore size, i.e. 2.5 μm for "A" and 2.2 μm for "S".

When introducing MWp or MWf into "S" polymer matrices, the scenario described previously for "A"-based membranes is maintained for "S"-based membranes, showing a flux increase for the membranes with 0.2 or 0.3 wt.% of MWp and that MWf is not beneficial in this type of membranes. However, the MWp load of 0.3 wt.% is better than 0.2 wt.%, in contrast with the results obtained with "A"-based membranes, that showed an optimal MWp load of 0.2 wt.%. This suggests the predominance of the beneficial effect of MWCNTs addition over the

viscosity increment, since MWCNTs addition increases membrane hydrophobicity, thermal stability and their smooth surface may enhance membrane permeability. In any case, the water flux obtained with 0.2MWp/A was much higher than that obtained with 0.3MWp/S and also considering the cost of MWCNTs one can conclude that the 0.2MWp/A membrane is a preferable option for DCMD.

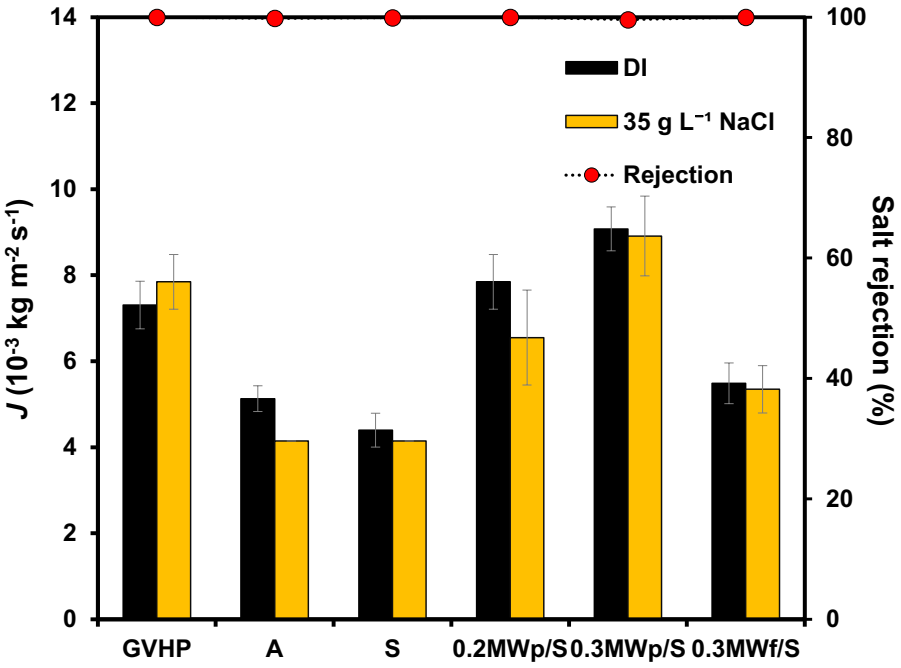

Figure 11. Effect of different PVDF types and MWCNTs addition on permeate flux and salt rejection in DCMD.

4. Conclusions

MWCNTs/PVDF blended membranes were prepared by the phase inversion method, studying different synthesis parameters such as MWCNTs loading and surface chemistry as well as PVP content. Increasing the loading of pristine carbon nanotubes (MWp), up to an optimum of 0.2 wt.% results in membranes with large pore sizes (determined by bubble point measurements), high pore density and sponge-like pores, also leading to the highest water flux

obtained with salty water (9.5×10^{-3} kg m^{-2} s^{-1}) while maintaining a complete salt rejection (i.e. 100 %) after 60 min.

PVP increased pore density, but at the same time produced elongated finger-like pores which have a negative effect on salt rejection at the employed conditions. Functionalization of MWCNTs (MWf) is not recommended for the preparation of this type of membranes due to the smaller pore size obtained by bubble point measurements, and respective lower water fluxes, in comparison to the equivalent membrane prepared by using MWp. It was also concluded that: (i) the thin top layer of the membrane has influence on the membrane permeability, through its pore size, pore distribution and hydrophobicity and, consequently, it should face the feed side solution (ALFS - active layer feed side configuration) to enhance the selective diffusion of vapour molecules through the membrane; (ii) the coagulation bath composition used to prepare the membranes also affects the water flux (water is preferable than a water/isopropyl alcohol solution); (iii) the mechanical resistance of the membranes can be increased by using polyester nonwoven supports without significantly affecting the membrane overall performance.

Therefore, flat-sheet MWCNTs/PVDF blended membranes with sponge-like pores and the lowest thickness possible (as that prepared by the phase inversion method using a DI water coagulation bath with 0.2 wt.% of MWp and without PVP), smaller pores and higher pore density at the top surface lead to higher water flux and complete salt rejection and, thus, they are good options for DCMD, in particular when compared with a commercially available PVDF membrane (GVHP from Millipore).

Acknowledgments

Financial support for this work was provided by project PTDC/AAC-AMB/122312/2010 co-financed by FCT (Fundação para a Ciência e a Tecnologia) and FEDER through Programe COMPETE (FCOMP-01-0124-FEDER-019503). This work was partially

supported by FCT and FEDER through project PEst-C/EQB/LA0020/2013 under Programe COMPETE, and by QREN, ON2 and FEDER through projects NORTE-07-0124-FEDER-0000015 and NORTE-07-0202-FEDER-038900. SMT acknowledges financial support from SFRH/BPD/74239/2010. AMTS acknowledges the FCT Investigator 2013 Programme (IF/01501/2013), with financing from the European Social Fund and the Human Potential Operational Programme.

References

[1] A.E. Ercin, A.Y. Hoekstra, Water footprint scenarios for 2050: A global analysis, Environment International, 64 (2014) 71-82.

[2] C.Z. Sun, M.S.H. Boutilier, H. Au, P. Poesio, B.F. Bai, R. Karnik, N.G. Hadjiconstantinou, Mechanisms of Molecular Permeation through Nanoporous Graphene Membranes, Langmuir, 30 (2014) 675-682.

[3] M. Khayet, Membranes and theoretical modeling of membrane distillation: A review, Advances in Colloid and Interface Science, 164 (2011) 56-88.

[4] M.M.A. Shirazi, A. Kargari, M. Tabatabaei, A.F. Ismail, T. Matsuura, Concentration of glycerol from dilute glycerol wastewater using sweeping gas membrane distillation, Chemical Engineering and Processing: Process Intensification, 78 (2014) 58-66.

[5] M.M.A. Shirazi, A. Kargari, D. Bastani, L. Fatehi, Production of drinking water from seawater using membrane distillation (MD) alternative: direct contact MD and sweeping gas MD approaches, Desalination and Water Treatment, 52 (2013) 2372-2381.

[6] M.M.A. Shirazi, A. Kargari, M. Tabatabaei, Evaluation of commercial PTFE membranes in desalination by direct contact membrane distillation, Chemical Engineering and Processing: Process Intensification, 76 (2014) 16-25.

[7] L. Camacho, L. Dumée, J. Zhang, J.-d. Li, M. Duke, J. Gomez, S. Gray, Advances in Membrane Distillation for Water Desalination and Purification Applications, Water, 5 (2013) 94-196.

[8] A. Alkhudhiri, N. Darwish, N. Hilal, Membrane distillation: A comprehensive review, Desalination, 287 (2012) 2-18.

[9] J.K. Holt, Fast mass transport through sub-2-nanometer carbon nanotubes, Science, 312 (2006) 1034-1037.

[10] G. Hummer, J.C. Rasaiah, J.P. Nowotyta, Water conduction through the hydrophobic channel of a carbon nanotube, Nature, 414 (2001) 188-190.

[11] A.F. Ismail, P.S. Goh, S.M. Sanip, M. Aziz, Transport and separation properties of carbon nanotube-mixed matrix membrane, Separation and Purification Technology, 70 (2009) 12-26.

[12] P.S. Goh, A.F. Ismail, B.C. Ng, Carbon nanotubes for desalination: Performance evaluation and current hurdles, Desalination, 308 (2013) 2-14.

[13] H.A. Shawky, S.-R. Chae, S. Lin, M.R. Wiesner, Synthesis and characterization of a carbon nanotube/polymer nanocomposite membrane for water treatment, Desalination, 272 (2011) 46-50.

[14] L. Dumée, K. Sears, J.r. Schü tz, N. Finn, M. Duke, S. Gray, Carbon nanotube based composite membranes for water desalination by membrane distillation, Desalination and Water Treatment, 17 (2010) 72-79.

[15] L. Dumée, V. Germain, K. Sears, J. Schütz, N. Finn, M. Duke, S. Cerneaux, D. Cornu, S. Gray, Enhanced durability and hydrophobicity of carbon nanotube bucky paper membranes in membrane distillation, Journal of Membrane Science, 376 (2011) 241-246.

[16] S. Morales-Torres, T.L.S. Silva, L.M. Pastrana-Martínez, A.T.S.C. Brandão, J.L. Figueiredo, A.M.T. Silva, Modification of the surface chemistry of single- and multi-walled

carbon nanotubes by HNO_3 and H_2SO_4 hydrothermal oxidation for application in direct contact membrane distillation, Physical Chemistry Chemical Physics, 16 (2014) 12237-12250.

[17] L.F. Dumée, K. Sears, J. Schütz, N. Finn, C. Huynh, S. Hawkins, M. Duke, S. Gray, Characterization and evaluation of carbon nanotube Bucky-Paper membranes for direct contact membrane distillation, Journal of Membrane Science, 351 (2010) 36-43.

[18] S.M. Sanip, A.F. Ismail, P.S. Goh, T. Soga, M. Tanemura, H. Yasuhiko, Gas separation properties of functionalized carbon nanotubes mixed matrix membranes, Separation and Purification Technology, 78 (2011) 208-213.

[19] M. Bhadra, S. Roy, S. Mitra, Enhanced desalination using carboxylated carbon nanotube immobilized membranes, Separation and Purification Technology, 120 (2013) 373-377.

[20] A.C.D. Morihama, J.C. Mierzwa, Clay nanoparticles effects on performance and morphology of poly(vinylidene fluoride) membranes, Brazilian Journal of Chemical Engineering, 31 (2014) 79-93.

[21] K. Smolders, A.C.M. Franken, Terminology for Membrane Distillation, Desalination, 72 (1989) 249-262.

[22] S. Brunauer, P.H. Emmett, E. Teller, Adsorption of gases in multimolecular layers, Journal of the American Chemical Society, 60 (1938) 309-319.

[23] F. Rouquerol, J. Rouquerol, K.S.W. Sing, Adsorption by Powders and Porous Solids. Principles, Methodology and Applications, in, Academic Press, London, 1999, pp. 219 – 228.

[24] L.M. Pastrana-Martínez, S. Morales-Torres, S.K. Papageorgiou, F.K. Katsaros, G.E. Romanos, J.L. Figueiredo, J.L. Faria, P. Falaras, A.M.T. Silva, Photocatalytic behaviour of nanocarbon-TiO_2 composites and immobilization into hollow fibres, Applied Catalysis B: Environmental, 142-143 (2013) 101-111.

[25] D. Hopkinson, M. Zeh, D. Luebke, The bubble point of supported ionic liquid membranes using flat sheet supports, Journal of Membrane Science, 468 (2014) 155-162.

[26] J. Yu, X. Hu, Y. Huang, A modification of the bubble-point method to determine the pore-mouth size distribution of porous materials, Separation and Purification Technology, 70 (2010) 314-319.

[27] J. Zhang, Z. Xu, M. Shan, B. Zhou, Y. Li, B. Li, J. Niu, X. Qian, Synergetic effects of oxidized carbon nanotubes and graphene oxide on fouling control and anti-fouling mechanism of polyvinylidene fluoride ultrafiltration membranes, Journal of Membrane Science, 448 (2013) 81-92.

[28] G.-d. Kang, Y.-m. Cao, Application and modification of poly(vinylidene fluoride) (PVDF) membranes – A review, Journal of Membrane Science, 463 (2014) 145-165.

[29] H.J. Kim, K. Choi, Y. Baek, D.-G. Kim, J. Shim, J. Yoon, J.-C. Lee, High-Performance Reverse Osmosis CNT/Polyamide Nanocomposite Membrane by Controlled Interfacial Interactions, ACS Applied Materials & Interfaces, 6 (2014) 2819-2829.

[30] M.M.A. Shirazi, D. Bastani, A. Kargari, M. Tabatabaei, Characterization of polymeric membranes for membrane distillation using atomic force microscopy, Desalination and Water Treatment, 51 (2013) 6003-6008.

[31] D. Chen, M. Wang, W.-D. Zhang, T. Liu, Preparation and characterization of poly(vinylidene fluoride) nanocomposites containing multiwalled carbon nanotubes, Journal of Applied Polymer Science, 113 (2009) 644-650.

[32] A. Rahimpour, S.S. Madaeni, S. Zereshki, Y. Mansourpanah, Preparation and characterization of modified nano-porous PVDF membrane with high antifouling property using UV photo-grafting, Applied Surface Science, 255 (2009) 7455-7461.

[33] M. Khayet, T. Matsuura, Membrane Distillation: Principles and Applications, Elsevier, 2011.

[34] L.F. Dumée, S. Gray, M. Duke, K. Sears, J. Schütz, N. Finn, The role of membrane surface energy on direct contact membrane distillation performance, Desalination, 323 (2013) 22-30.

[35] A. Razmjou, E. Arifin, G. Dong, J. Mansouri, V. Chen, Superhydrophobic modification of TiO_2 nanocomposite PVDF membranes for applications in membrane distillation, Journal of Membrane Science, 415–416 (2012) 850-863.

[36] D. Winter, J. Koschikowski, D. Düver, P. Hertel, U. Beuscher, Evaluation of MD process performance: Effect of backing structures and membrane properties under different operating conditions, Desalination, 323 (2013) 120-133.

[37] F. Liu, N.A. Hashim, Y. Liu, M.R.M. Abed, K. Li, Progress in the production and modification of PVDF membranes, Journal of Membrane Science, 375 (2011) 1-27.

[38] B.S. Lalia, V. Kochkodan, R. Hashaikeh, N. Hilal, A review on membrane fabrication: Structure, properties and performance relationship, Desalination, 326 (2013) 77-95.

[39] E. Fontananova, J.C. Jansen, A. Cristiano, E. Curcio, E. Drioli, Effect of additives in the casting solution on the formation of PVDF membranes, Desalination, 192 (2006) 190-197.

[40] E. Saljoughi, M. Amirilargani, T. Mohammadi, Effect of poly(vinyl pyrrolidone) concentration and coagulation bath temperature on the morphology, permeability, and thermal stability of asymmetric cellulose acetate membranes, Journal of Applied Polymer Science, 111 (2009) 2537-2544.

[41] M.A. Tofighy, T. Mohammadi, Salty water desalination using carbon nanotube sheets, Desalination, 258 (2010) 182-186.

[42] J.-H. Choi, J. Jegal, W.-N. Kim, Fabrication and characterization of multi-walled carbon nanotubes/polymer blend membranes, Journal of Membrane Science, 284 (2006) 406-415.

[43] S. Bonyadi, T.-S. Chung, Highly porous and macrovoid-free PVDF hollow fiber membranes for membrane distillation by a solvent-dope solution co-extrusion approach, Journal of Membrane Science, 331 (2009) 66-74.

[44] K. Gethard, O. Sae-Khow, S. Mitra, Carbon nanotube enhanced membrane distillation for simultaneous generation of pure water and concentrating pharmaceutical waste, Separation and Purification Technology, 90 (2012) 239-245.

[45] K. Gethard, O. Sae-Khow, S. Mitra, Water Desalination Using Carbon-Nanotube-Enhanced Membrane Distillation, ACS Applied Materials & Interfaces, 3 (2010) 110-114.

[46] W.-S. Bae, O. Kwon, B. Kim, D. Chae, Effects of multi-walled carbon nanotubes on rheological and physical properties of polyamide-based thermoplastic elastomers, Korea-Aust. Rheol. J., 24 (2012) 221-227.

[47] V. Vatanpour, S.S. Madaeni, R. Moradian, S. Zinadini, B. Astinchap, Fabrication and characterization of novel antifouling nanofiltration membrane prepared from oxidized multiwalled carbon nanotube/polyethersulfone nanocomposite, Journal of Membrane Science, 375 (2011) 284-294.

[48] P.S. Goh, A.F. Ismail, S.M. Sanip, B.C. Ng, M. Aziz, Recent advances of inorganic fillers in mixed matrix membrane for gas separation, Separation and Purification Technology, 81 (2011) 243-264.

[49] R.R.N. Marques, B.F. Machado, J.L. Faria, A.M.T. Silva, Controlled generation of oxygen functionalities on the surface of Single-Walled Carbon Nanotubes by HNO3 hydrothermal oxidation, Carbon, 48 (2010) 1515-1523.

[50] A.M.T. Silva, B.F. Machado, J.L. Figueiredo, J.L. Faria, Controlling the surface chemistry of carbon xerogels using HNO3-hydrothermal oxidation, Carbon, 47 (2009) 1670-1679.

[51] B. Corry, Water and ion transport through functionalised carbon nanotubes: implications for desalination technology, Energy & Environmental Science, 4 (2011) 751-759.

[52] G.V.P. Ramana, Balaji; Kumar, R Naresh; Prabhakar, K V P; Jain, P K, Mechanical properties of multi-walled carbon nanotubes reinforced polymer nanocomposites, Indian Journal of Engineering and Materials Sciences, 17 (2010) 331-337.

[53] A. Figoli, S. Simone, A. Criscuoli, S.A. Al-Jlil, F.S. Al Shabouna, H.S. Al-Romaih, E. Di Nicolò, O.A. Al-Harbi, E. Drioli, Hollow fibers for seawater desalination from blends of PVDF with different molecular weights: Morphology, properties and VMD performance, Polymer, 55 (2014) 1296-1306.

[54] J.Y. Han, H.-H. Oh, K. Jun Choi, B.R. Min, Characterization of poly(vinylidene fluoride) flat sheet membranes prepared in various ratios of water/ethanol for separator of li-ion batteries: Morphology and other properties, Journal of Applied Polymer Science, 122 (2011) 2653-2665.